10

Use of Visible Geostationary Operational Meteorological Satellite Imagery in Mapping Reference and Potential Evapotranspiration over Florida

John R. Mecikalski[1], David M. Sumner[2], Jennifer M. Jacobs[3], Chandra S. Pathak[4], Simon J. Paech[5], and Ellen M. Douglas[6]
[1]*University of Alabama in Huntsville, Huntsville, Alabama*
[2]*U. S. Geological Survey (USGS), Orlando, Florida*
[3]*University of New Hampshire, Durham, New Hampshire*
[4]*South Florida Water Management District, West Palm Beach, Florida*
[5]*University of Alabama in Huntsville, Huntsville, Alabama*
[6]*University of Massachusetts, Boston, Massachusetts*
USA

1. Introduction

In Florida, the fraction of mean, annual precipitation returned to the atmosphere as evaporation and transpiration ranges from ~50% in settings of relatively deep water table, shallow-rooted vegetation, and sandy soils (Sumner, 2001) to almost 110% from lakes (Swancar et al., 2000). The prominence of evapotranspiration (ET) in Florida water budgets necessitates its quantification for reliable water-resources management. Water-resources planning often requires use of hydrologic models to assess the impact (e.g., reduction in streamflows, wetland dehydration, or salt-water intrusion into an aquifer) of possible stresses to a hydrologic system. Hydrologic models require spatial and temporal quantification of fluxes into and out of the hydrologic system. The prominence of the outgoing ET flux within the water budget dictates that this flux must be included in many hydrologic models. As actual ET (AET) data are often lacking, ET is usually implemented within hydrologic models with a specified potential ET (PET), defined as the maximum ET at a given location in the absence of water stress, and a conceptualization of the relation between AET and PET. Water allocation and crop use requirements are often estimated using reference ET (RET) and crop coefficients. RET is defined as the ET from a standard reference crop of either grass or alfalfa. In Florida, an assumption of a hypothetical 12-cm grass reference is commonly used; the grass is assumed to be dense and actively growing. RET is typically computed at specific locations based on weather station data.

Estimates of incoming solar radiation (insolation, or R_s) have been made from geostationary satellite data over a 14-year period (1 June 1995 to 31 December 2009, continuing) for use by State of Florida Water Management Districts in ET estimation (Paech et al., 2009). Clearly, geostationary satellites provide spatially and temporally continuous data across all regions

in their view (between ±55° latitude), a major advantage over ground-based instrumentation. The most desirable ET datasets are spatially continuous, rather than point values derived from traditional weather station networks. Thus, Statewide mapping of ET is greatly facilitated by satellite-derived estimates of the spatial distribution of insolation. Use of a satellite-based insolation algorithm also ensures that a consistent algorithm is applied across an entire region. Insolation is the primary determinant for temporal variation in PET and RET and is also a large determinant of spatial variation in these values, particularly in areas with heterogeneous cloud cover. RET is valuable for irrigation scheduling and water management, and PET can be used as input into surface and groundwater hydrological models, whereas the insolation data themselves may be used as data input in certain ecosystem models. The five Florida Water Management Districts have not had access to consistent, spatially continuous methods of computing RET and PET. A robust insolation calibration framework coupled to a satellite-based insolation model is described, toward providing a key radiative dataset for the formulation of an initial 9.5-year long (June 1995 - December 2004) ET climatology (which has subsequently been extended through 2009, with annual updates). These insolation datasets are used in conjunction with other information, such as net radiation (R_N), air temperature, relative humidity, wind speed, and land cover information in the formulation of daily, 2-km estimates of PET and RET throughout Florida.

2. GOES insolation data

Satellite visible data have been used for estimating insolation for a number of years, with methods ranging from statistical-empirical relations such as Tarpley (1979), to physical models of varying complexity (see Gautier et al., 1980; Diak & Gautier, 1983; Gautier et al. 1984; Möser & Raschke, 1984; Pinker & Ewing, 1985; Dedieu et al., 1987; Darnell et al., 1988; Frouin & Chertock, 1992; Pinker & Laszlo, 1992; Weymouth & Le Marshall, 1999). Studies such as Schmetz (1989) and Pinker et al. (1995) have proven the utility of satellite-estimated insolation methods, showing that such models produce fairly accurate results – with hourly insolation estimates within 5-10% of pyranometer data during clear-sky conditions (15-30% for all sky conditions) and daily all-sky estimates within 10-15%. Additional works such as those of Stewart et al. (1999) and Otkin et al. (2005) have further bolstered the utility of this technique. Advantages of using satellite-estimated insolation data over those collected by pyranometer networks include large spatial coverage, high spatial resolution, the availability of data in remote, inaccessible, or potentially hazardous regions, over oceans and large water bodies (e.g., Frouin et al., 1988), and in countries that may not have the means to install a ground-based pyranometer network. Cosgrove et al. (2003a,b) describes the use of the Global Energy and Water Cycle Experiment (GEWEX) Surface Radiation Budget (SRB) downward solar flux algorithm [Pinker & Laszlo, 1992] as demonstrated within the North American Land Data Assimilation (NLDAS) project. The error statistics for the SRB product are comparable to those shown by Paech et al. (2009), while the resolution of the SRB solar flux data are 0.5° (Meng et al., 2003).

Approximately 182,000 individual GOES images from the National Oceanic and Atmospheric Administration (NOAA) Geostationary Operational Environmental Satellite (GOES) "East" series of satellites were processed and used for this effort as of 31 December 2009. These data were processed using the method of Gautier et al. (1980) to produce half-hourly and daily-integrated insolation, and 2-week running noontime minimum surface albedo data throughout the State of Florida at 2-km horizontal spatial resolution. This 2 km

resolution is chosen to provide insolation observations between cumulus clouds, which make up a significant component of Florida's cloud climatology.
Following the data collection and processing, an extensive calibration activity for the insolation product was undertaken by comparing satellite-derived insolation estimates to ground-based pyranometer measurements and clear-sky radiation models. This comparison allowed for bias corrections to be applied to the daily-integrated insolation dataset for local environmental conditions. Bias corrections were achieved using a three-step process: (1) comparison with ground-based pyranometer measurements on clear (non-cloudy) "reference" days, (2) correcting for bias related to cloudiness, and (3) deriving a monthly bias correction factor. This resulted in a significant reduction in bias errors and henceforth the development of a robust ET product (for RET and PET).
Described in this chapter are the production and calibration of the 2 km GOES-based insolation product, along with the methodology for obtaining PET and RET.

2.1 The insolation model

The insolation estimation method developed by Gautier et al. (1980), with modifications by Diak & Gautier (1983) and updated application methods by Diak et al. (1996), is referred to as the Gautier-Diak-Masse (GDM) method, and employs a simple model representing cloud and atmosphere radiative processes. The GDM method has been shown to perform as well as, or even better than, more complex methods over a variety of land-surface and climatic conditions (Gautier et al., 1984; Frouin et al., 1988; Raphael & Hay, 1984; Diak et al., 1996; Jacobs et al., 2002, 2004; Otkin et al., 2005). Compared to pyranometer data, these studies reported root mean square errors in hourly and daily insolation estimates (as a percentage of the mean pyranometer observed value) from 17-28% and 9-10%, respectively. The high ends of these errors (~28% and ~10%, respectively) were reported in the study by Jacobs et al. (2002), which took place over north and central Florida and was characterized by significant convective-cloud activity. The GDM method has also been proven in operational use, producing near-real-time insolation estimates for regional- and continental-scale land-surface carbon, energy and water flux assessments (Mecikalski et al., 1999; Anderson et al., 2003, 2004), subsurface hydrologic modeling, and the generation of agricultural forecasting products (Diak et al., 1998; Anderson et al., 2001). A full description of the GDM is given by Gautier et al. (1980), Diak & Gautier (1983) and Diak et al. (1996) – a basic overview is given here.
The GDM method is based on conservation of radiant energy in the Earth-atmosphere column. The method has two modes for determining insolation received at the Earth's surface: one for clear and one for cloudy conditions, based on satellite-derived surface albedo (α) data. A running 2 week minimum of this α data, reassessed at solar noon daily, is stored for each GOES satellite visible data pixel, yielding a reference α grid representative of clear-sky conditions and capturing temporal changes in land-surface characteristics. This approach represents the true land-surface α more accurately than using the daily estimated value because the latter can be corrupted by high α values when clouds are present during the course of a day. This minimum α is wavelength-specific, unique to the GOES visible sensor (which does in fact include contributions from the near infrared), and therefore does not represent a true surface α.
Within the GDM, for a given GOES image, the digital brightness at each image pixel is compared to that of the stored clear-sky reference α data for that pixel. If the brightness

exceeds a given threshold [a function of the 2-week running minimum noontime α; Diak & Gautier, (1983)], the pixel is deemed cloudy, otherwise it is varying degrees of partly cloudy to clear. Based on this determination, either a clear or cloudy model of atmospheric radiation processes is used to calculate insolation received at the surface for each pixel. Both clear and cloudy models incorporate parameterizations for ozone absorption, Raleigh scattering, and water vapor absorption within the atmospheric column using simple bulk relations – the use of fixed ozone and aerosol contents being sufficient given that these produce secondary sources of error. The cloudy-sky component GDM method estimates a cloud-top α, and accounts for atmospheric effects above and below the cloud separately.

For the water vapor absorption parameterization, a fixed, approximate annual median value of 3.0 cm was used to estimate atmospheric column-integrated precipitable water (PW) during the initial processing. PW is the amount of water that would precipitate out of a vertical column of the atmosphere if all the water vapor were condensed into liquid. PW data are needed to calculate the slantwise path, and, subsequently, the absorption coefficients in the GDM method. Post-processing adjustments were then made to account for day-to-day variations of precipitable water (i.e. PW values greater or less than the 3.0 cm median value), given the logistical difficulty of including these data within the modeling stage. These adjustments were made by deriving adjustment factors based on daily representative PW values over Florida from numerical weather prediction model data. In many instances, daily PW values over Florida were well above 3.0 cm, especially during summer, while wintertime values were often much lower. No accounting was made for intra-day variations in PW considering the relatively small amount of variability that typically occurs over Florida, especially during summer, and because this would have required a reliance on forecasts from numerical weather prediction models, which are often incorrect. We also did not account for meso-γ scale (2-25 km) variations in PW given that such variations are most often quite small (<5%).

2.2 GOES data processing and quality control

The GOES East series of satellites (the most recent additions being GOES–8, –12 and –13) have been placed in geostationary orbit above the Earth's equator at longitude 75° W since 1975. These satellites provide continuous observations in visible and infrared radiation bands of much of the western hemisphere at high spatial (≥1 km) and temporal (≥15 min) resolution, making data collected by them ideal for high-resolution estimates of insolation. The GOES–8 satellite was launched in April 1994, became operational in late May 1995, and was replaced by GOES–12 on 1 April 2003. Subsequently, GOES–13 became operational on 15 April 2010. The Florida insolation processing began on 1 June 1995.

Although the GOES visible sensors have a nadir (the point directly below the satellite) spatial resolution of 1 km, this resolution decreases the farther from nadir the instrument scans. For the State of Florida, the highest resolution attainable is about 1.5-2.0 km, which was the input and output resolution of the GDM in this analysis. Half-hourly insolation values were calculated using GOES data from 15 and 45 min past the hour, and daily values were calculated by integrating the half-hourly values over the period of daylight using the trapezoidal integration method. A simple method for computing sunrise and sunset times per pixel across the domain was used. The running 2-week minimum α was calculated using data at solar noon. The original insolation and α fields, in satellite projection, were

then translated to a 2 x 2 km grid that has been used for the statewide NEXRAD radar-derived rainfall estimation product (Hoblit et al., 2003).

Potential GOES data quality issues include sensor degradation with time and sun glint effects. The effects of the latter are small. Sensor degradation is addressed and corrected through the calibration of the product, detailed in following sections. In general, GOES satellite data have high reliability. Under specific conditions, however, the instruments are shut down (for example, when sunlight shines directly into the sensors), and other issues such as receiving-station problems can result in the occasional loss or corruption of an image or series of images. For this reason, if more than 5 half-hourly satellite images are missing on a given day, the daily insolation value for that day was flagged as "unusable." Days with 3-5 missing images are designated "usable," and those with zero to two missing images are designated as "good quality" data. Gaps in the usable data were filled by linear interpolation.

3. Pyranometer data

Pyranometer data used to calibrate the GOES satellite isolation product, and subsequently assess calibration performance, were obtained from five weather station networks across Florida, each maintained by a different agency. The State of Florida is divided into five regional Water Management Districts (WMDs): Northwest Florida (NWF), South Florida (SF), St. Johns River (SJR), Suwannee River (SR), and Southwest Florida (SWF). Historical pyranometer data were provided by three of the WMDs (SF, SJR, and SWF), and the remaining data were obtained from the University of Florida (UF) Institute of Food and Agricultural Sciences (IFAS) Florida Automated Weather Network (FAWN; fawn.ifas.ufl.edu), and from a single long-term station operated by the U. S. Geological Survey (USGS). Data from 57 stations were used; with stations divided into three groups, "Group 1," "Group 2," and "Group 3". Group 1 stations were used for GDM performance assessment (validation), and Group 2 and 3 data were used for calibration. For performance assessment (Group 1), we used nine stations – two within each WMD (except NWF, where only one quality station was available) so that each part of the State would be represented. Group 1 stations had good data quality over the longest periods of record. For Groups 2 and 3, high-quality data also were needed, but many different stations were used over the initial 10-year period (1995-2004) of analysis. Figure 1 shows the locations of all stations within groups over Florida.

Each weather station network used the LI-200 pyranometer produced by LI-COR, Inc. (Lincoln, NE), with recalibration performed every 1-2 years and quoted accuracy of <5%. Pyranometer locations varied from open fields to water bodies (lakes), but saltwater settings were avoided whenever possible in this calibration effort to minimize issues such as salt deposit contamination of the sensors. Temporal resolution of the pyranometer data ranged from 15 min to 1 hr averages, and daily-integrated insolation values were calculated using the midpoint integration method.

A practical issue for the calibration of satellite-based estimates of insolation is the availability of good quality pyranometer data. Most of the data were provided with quality assurance and quality control (QA/QC) flags, but these flags were not adequate for our purposes. Hence, an additional method for evaluating the data, developed by the American Society of Civil Engineers (ASCE), was employed (see Allen et al., 2005). This method involved comparing daily-integrated insolation data (half-hourly insolation data integrated

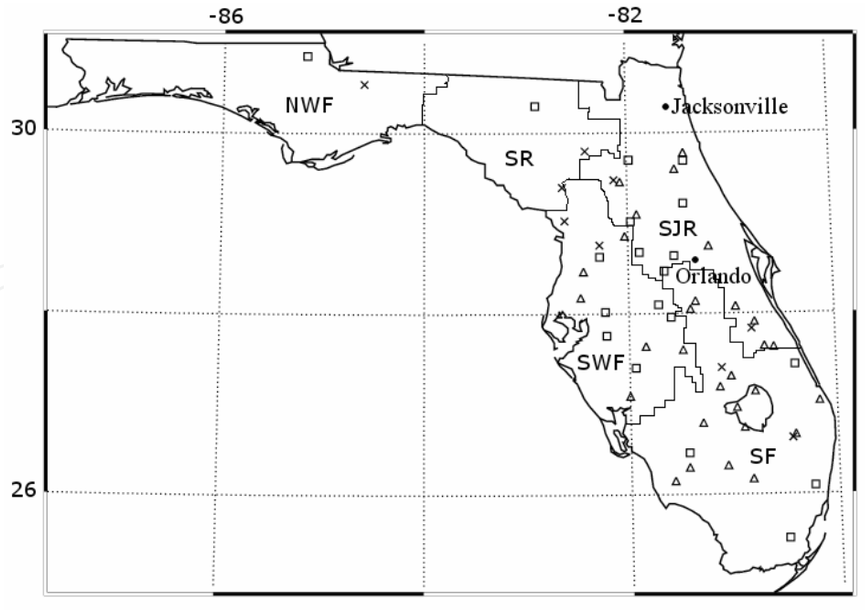

Fig. 1. Locations of pyranometer stations used in GDM calibration. Group 1, 2 and 3 datasets are denoted by crosses, triangles, and squares, respectively. State boundaries and WMD region boundaries are thick and thin black lines, respectively. WMD acronyms are shown. Latitudes are given on the left side and longitudes at the top. Lake Okeechobee can be seen in the southeast part of the state.

into one daily total) with estimated clear-sky radiation, R_{so} (MJm^{-2}day^{-1}), estimated as a function of station elevation (z) and extraterrestrial radiation (R_a: short-wave solar radiation in the absence of an atmosphere) over a 24-hour period by

$$R_{so} = (0.75 + 2 \times 10^{-5} z) R_a \,, \tag{1}$$

where R_a is a function of day of year, solar constant, solar declination, and latitude, given by

$$R_a = \frac{24}{\pi} G_{sc} d_r [\omega_s \sin(\varphi)\sin(\delta) + \cos(\varphi)\cos(\delta)\sin(\omega_s)] \,. \tag{2}$$

Here, G_{sc} is the solar constant (4.92 MJm^{-2}h^{-1}), d_r is the inverse relative distance factor for the Earth-Sun (unitless), ω_s is the sunset hour angle (radians), φ is latitude (radians), and δ is the solar declination (radians) (Duffie & Beckman, 1980; Allen, 1996; Allen et al., 2005).

The assumption is that measured daily insolation should be close to estimated clear-sky values on at least some days during the year – those days being considered "cloud-free." When examining annual plots of both measured and cloud-free insolation, it was possible to identify when a station had significant data quality issues not indicated by QA/QC flags; specifically, under complete sunshine, quality pyranometer measurements should be near the R_{so} values. For pyranometer data not provided with any QA/QC information, the above method was employed as an initial filter, following that, data greater than 105% of the estimated clear-sky value were removed (Allen et al., 2005). Periods of the record, or even entire station records, that had measured values either substantially above or below the cloud-free "envelope" (by ≥5%) were eliminated from analysis.

4. GDM method calibration for insolation data

The GDM method performs well over a variety of land-surface and climatic conditions, as well as over a range of spatial and temporal resolutions. However, daily-integrated GOES-estimated insolation has biases that can be reduced by adjustments for clear sky conditions, cloudy sky conditions, and seasonality. GOES insolation estimates were fine-tuned through a cumulative three-step process by calibration to ground-based pyranometer data. In this section, we will discuss each of these bias corrections in detail. Briefly, the initial insolation data that are estimated from the GDM method (referred to as the "DAILY_A" dataset) were compared with pyranometer observations on clear (non-cloudy) reference days, resulting in a set of initial calibration coefficients, the application of which produced the second "DAILY_B" dataset. Then, a "cloudiness" bias correction was determined and applied to the DAILY_B data, resulting in the "DAILY_C" dataset. Lastly, a monthly correction factor was applied to the DAILY_C data, yielding the final dataset "DAILY_D". At each calibration step, GOES-estimated and pyranometer-measured insolation data were matched spatially by choosing the satellite data pixel that corresponded to the location of the pyranometer station.

To assess the performance of each calibration step, the A, B, C, and D datasets were compared to data from the "Group 1" stations, which were nine independent stations not used in the calibration process. The results of each step are shown for the entire data period and each of the nine stations in Fig. 2. Statistics used for this comparison included on each plot are the Root Mean Square Error (RMSE, also expressed as a percentage of the mean pyranometer observed value), the Mean Bias Error (MBE), and the coefficient of determination (r^2). Figure 3a shows station-averaged statistics and seasonal-station averaged GDM MBE. The number of stations in the averaged statistics (Fig. 3b) varied from 2 to 7 depending on the length of record for each station.

4.1 Clear day comparison

Disparities between satellite-estimated and pyranometer-measured insolation on clear-sky days should be at a minimum, because without clouds, insolation received at the surface will be spatially homogeneous, providing reference conditions for the comparison of the two datasets. These "clear day comparisons" were made every 6 month on days as free of cloud as possible over Florida – one day in each summer and winter season. Clear days over the entire State of Florida are rare, and therefore many times the comparison was limited to available cloud-free regions.

For each clear day, the half-hourly GDM data were compared with pyranometer data for up to three "Group 2" stations within each of the SF, SJR and SWF WMD regions (no data were available for NWF or SR for this analysis). Pyranometer time-stamps were adjusted to the middle of their data-averaging periods, and paired with unmodified GOES data times on the top of the hour and half-hour. For each WMD region that was analyzed, the GDM and corresponding pyranometer datasets were averaged across the selected stations, resulting in two diurnal curves (one each for the GDM and pyranometer). These two averaged datasets were then compared over the same 24-hour periods, and the satellite data calibration coefficient for each WMD was determined by multiplying the averaged GDM satellite data by a factor necessary for its diurnal insolation curve to closely align with the averaged pyranometer curve. This factor was manually determined as a means of correcting for the satellite–pyranometer differences in clear sky radiation.

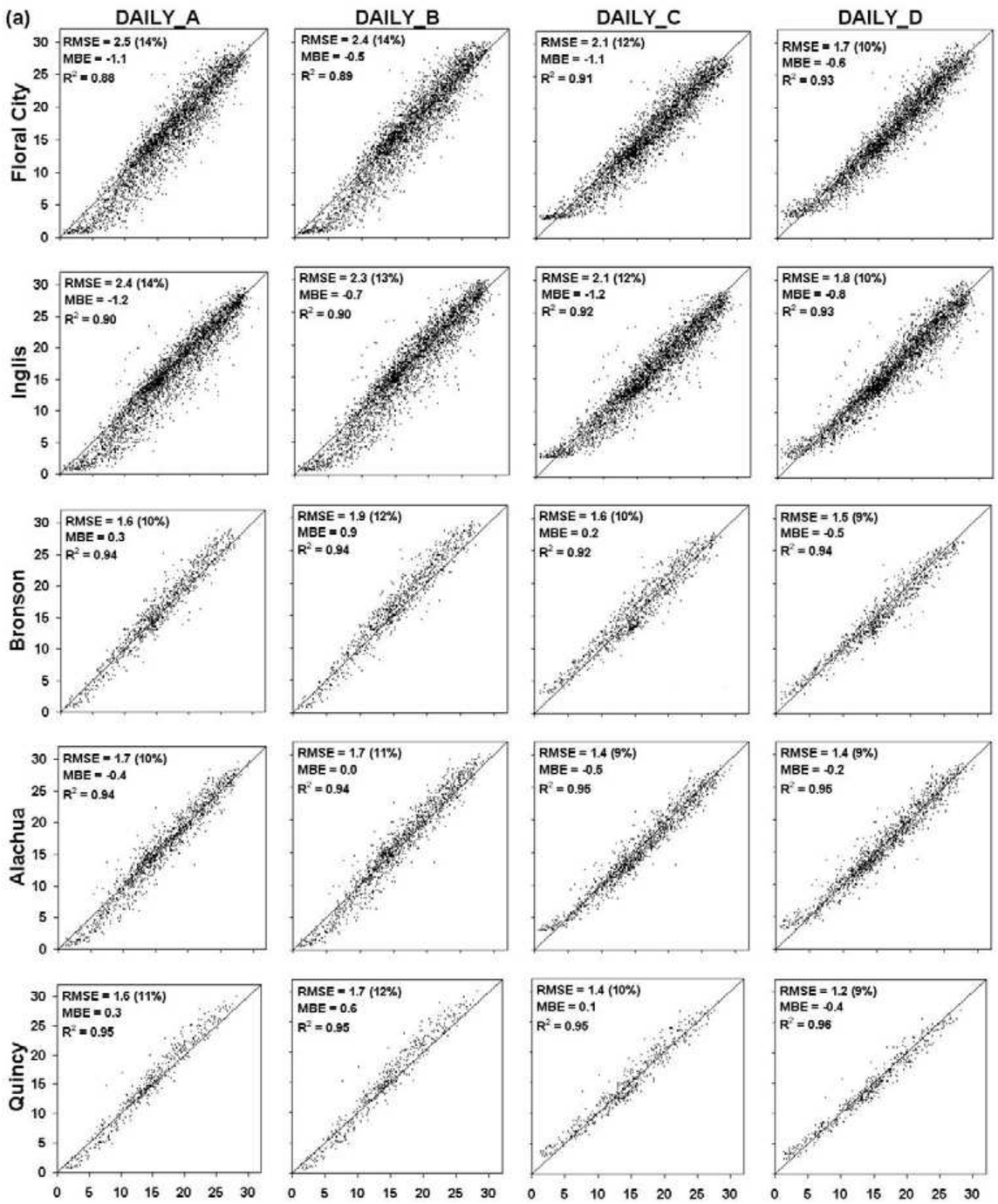

Fig. 2. Comparison of satellite-estimated (ordinate) and pyranometer-measured (abscissa) daily integrated insolation [$MJm^{-2}day^{-1}$] for the nine model calibration locations. Station names are given along the left-side, and comparison satellite-estimated dataset names are given at the top. RMSE values [$MJm^{-2}day^{-1}$], RMSE as a percentage of the mean observed value (in parentheses), MBE [$MJm^{-2}day^{-1}$], and coefficient of determination (R^2 as in figures) for each station and calibration step combination also are shown.

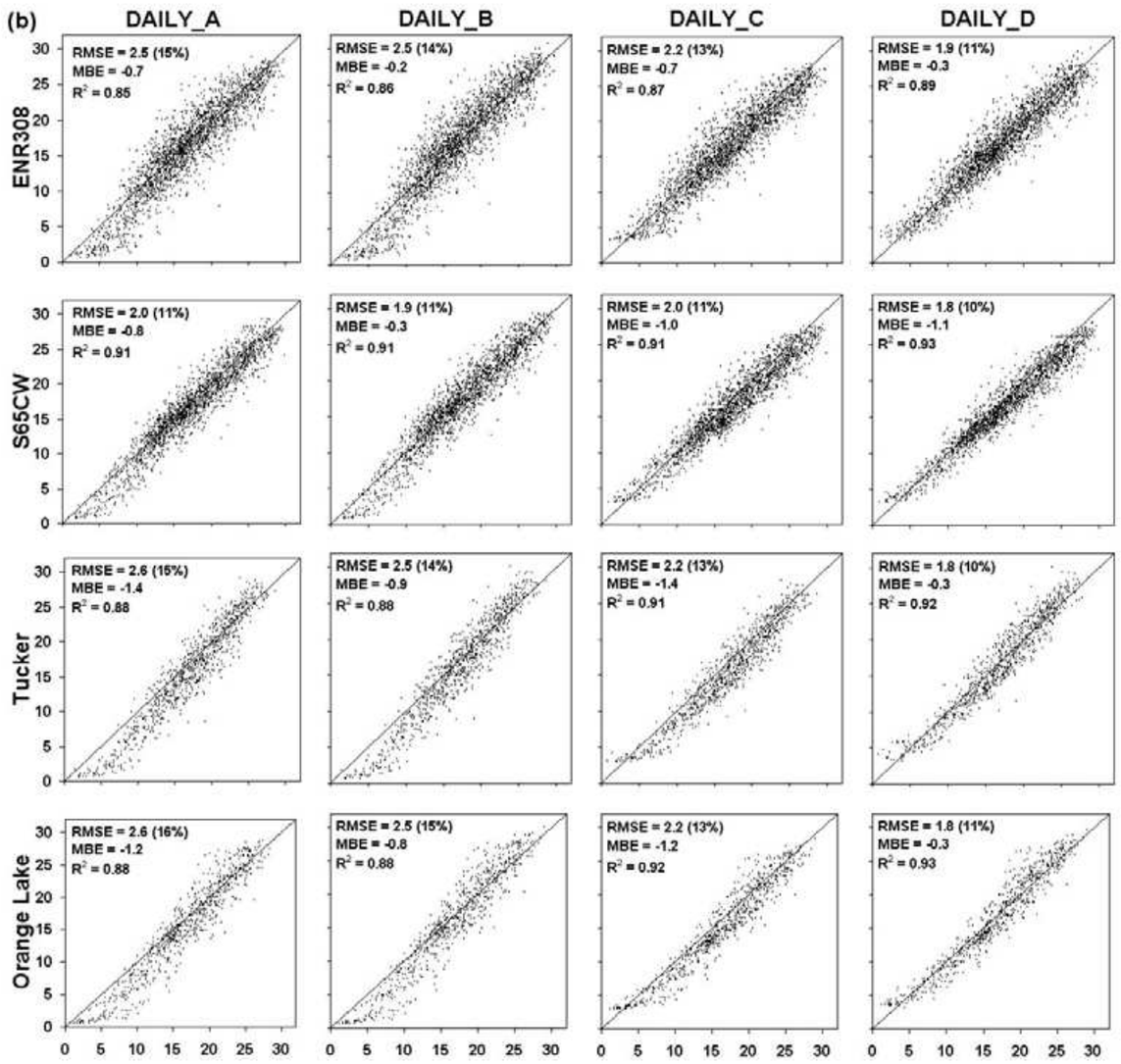

Fig. 2. Continued.

Subsequently, the average of all available WMD correction factors was taken to obtain a calibration coefficient for that particular day to apply over the entire State of Florida. This process was carried out for the entire observation period, resulting in a set of 20 approximately bi-annual clear sky calibration coefficients spanning the data record. The individual coefficients, obtained only on days when pyranometer data were available, were then interpolated in time to obtain a calibration coefficient set that could be applied to each day across the data record.

For calibration of the GDM, the clear sky coefficients were applied to the initial (DAILY_A) data, yielding the DAILY_B dataset. The results of this calibration are shown in Fig. 2 and indicate that the 9-station averaged RMSE remained the same as that of the DAILY_A dataset, the coefficient of determination increased to 0.91, and the average MBE decreased in magnitude from –0.7 to –0.2 $MJm^{-2}day^{-1}$. Figure 3a shows that after the correction for clear sky bias, the MBE generally has been reduced, but a temporal trend of MBE (positive shift with time) is present, and the station and seasonal averages have a similar range (beginning

to end) as the initial DAILY_A dataset. A seasonal MBE oscillation is also evident, as is a cloudiness-related bias (Fig. 2).

4.2 Cloudiness bias correction

In an effort to correct for a known cloudiness-related bias in GDM data, a "cloudiness" bias correction was developed using the DAILY_B satellite-estimated insolation dataset (the result of the clear-day calibration). These data were compared with pyranometer data from the "Group 3" dataset with GDM bias values calculated for each individual station and day, and plotted versus "cloudiness index". The cloudiness index is defined here as the ratio of the DAILY_B satellite-estimated insolation to estimated daily clear-sky insolation, R_{so}. The model bias due to cloudiness [$MJm^{-2}day^{-1}$] is approximately linearly related to cloudiness by

$$Cloudiness\_bias = 4.44[Cloudiness\_index] - 2.55 \quad (3)$$

The cloudiness bias given by Eq. (3) was calculated for each Group 3 station for all days and subtracted from the DAILY_B data, resulting in the DAILY_C dataset. Examination of the DAILY_C dataset revealed that the bias related to cloudiness was almost negligible, leading to an increase in the coefficient of determination from 0.91 to 0.92 and a decrease in the average RMSE from 2.2 to 1.9 $MJm^{-2}day^{-1}$. This small improvement is also evident in Fig. 2; although the low end of the model data has been "raised" somewhat, this affects only a small percentage of the data. For the ultimate purpose of this dataset, which is the estimation of ET in Florida, correcting for the cloudiness bias has a small effect seen primarily on very cloudy days, when ET is typically low. With the cloudiness bias correction, the station and time-averaged MBE becomes more negative and increases in magnitude from –0.2 to –0.8 $MJm^{-2}day^{-1}$ (Fig. 3).

4.3 Monthly bias correction and final insolation product

The final calibration step was the development of a monthly bias correction. DAILY_C model and "Group 3" pyranometer data were averaged over all calibration stations for each month. The pyranometer data were then subtracted from the DAILY_C data, resulting in a set of monthly bias correction coefficients spanning the data period. Due to data availability and time constraints, June 1996 through June 1997 coefficients were used for the June 1995 through June 1996 period. This was deemed acceptable as the most important bias features (for example the seasonal oscillation) were captured by this surrogate set of coefficients. These bias corrections were then subtracted from the DAILY_C data, giving us the final dataset, DAILY_D (as shown in Figs. 2 and 3).

The result of all bias corrections was that the station-averaged statistics all improved. The average RMSE and MBE values decreased in magnitude to 1.7 (10% of the mean observed value) and –0.5 $MJm^{-2}day^{-1}$, respectively, and the coefficient of determination increased to 0.93. Compared to the initial dataset (DAILY_A), the RMSE and MBE decreased in magnitude by 0.5 and 0.2 $MJm^{-2}day^{-1}$, respectively, and the coefficient of determination increased by 0.03. Although the final average MBE is still negative and of greater magnitude than the result of the DAILY_B calibration, Fig. 3 shows that the effect of the monthly bias correction led to the removal of both the seasonal oscillation and the positive shift of MBE with time, with the final station average ranging between about –1 to 0 $MJm^{-2}day^{-1}$ across the data record period compared to DAILY_A. Lower GOES insolation values (from 0 to 3

MJm^{-2}day^{-1}) were completely removed during the calibration process, as evident in all DAILY_C and DAILY_D datasets.

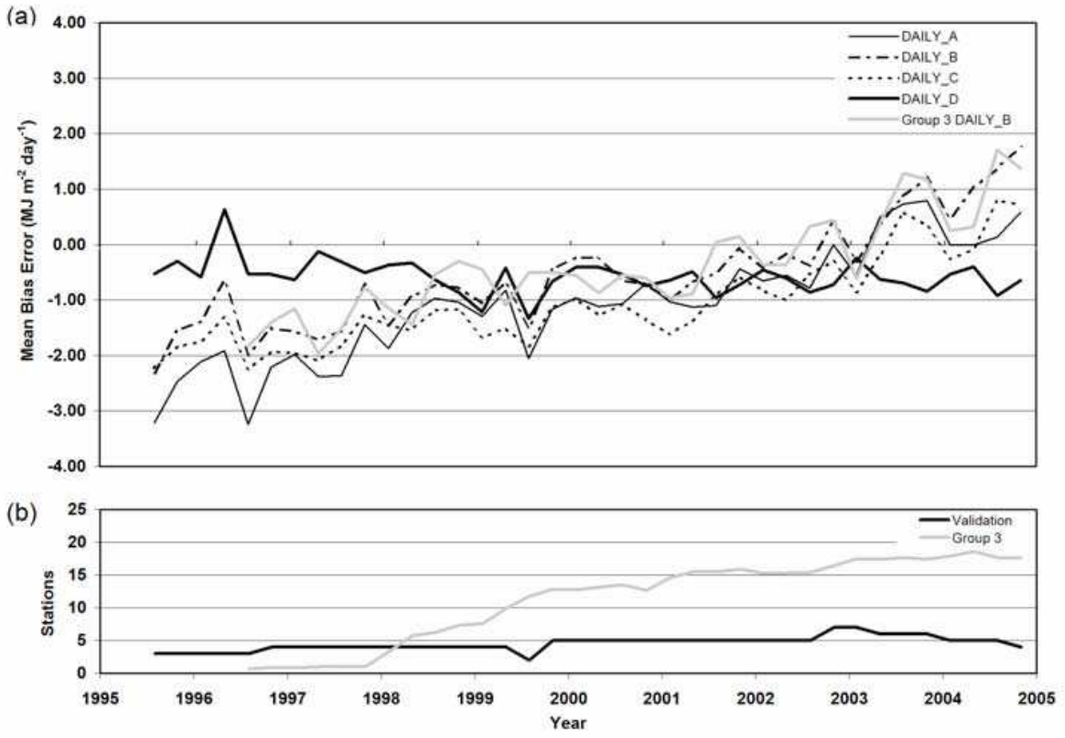

Fig. 3. (a) Season and station averaged daily integrated insolation MBE, and (b) number of stations in the average at any given time. The "Group 3" dataset is included in both (a) and (b) for comparison. Season months are December to February (winter), March to May (spring), etc.

5. Estimating potential ET

5.1 Utility of potential ET methods

Numerous methods exist to estimate PET using atmospheric parameters including wind speed, net radiation (R_N), temperature, and relative humidity (Vörösmarty et al., 1998; Oudin et al., 2005). The study by Douglas et al. (2009) used observed daily ET (DET) from 18 sites in Florida having measured DET and ancillary climate data to compare the performance of three common methods for estimating PET: the Turc, the Priestley–Taylor, and the Penman–Monteith methods. The sites were distributed throughout the State of Florida and represent a variety of land cover types: open water, marshland, grassland/pasture, citrus, and forest. The performance of the three methods when applied to conditions close to PET was used to judge relative merit. Under such PET conditions, the annually aggregated Priestley–Taylor and Turc methods performed comparably across land covers, and outperformed the Penman–Monteith method, possibly due to the use of generic literature values for coefficients in the Penman–Monteith method (Douglas et al., 2009).

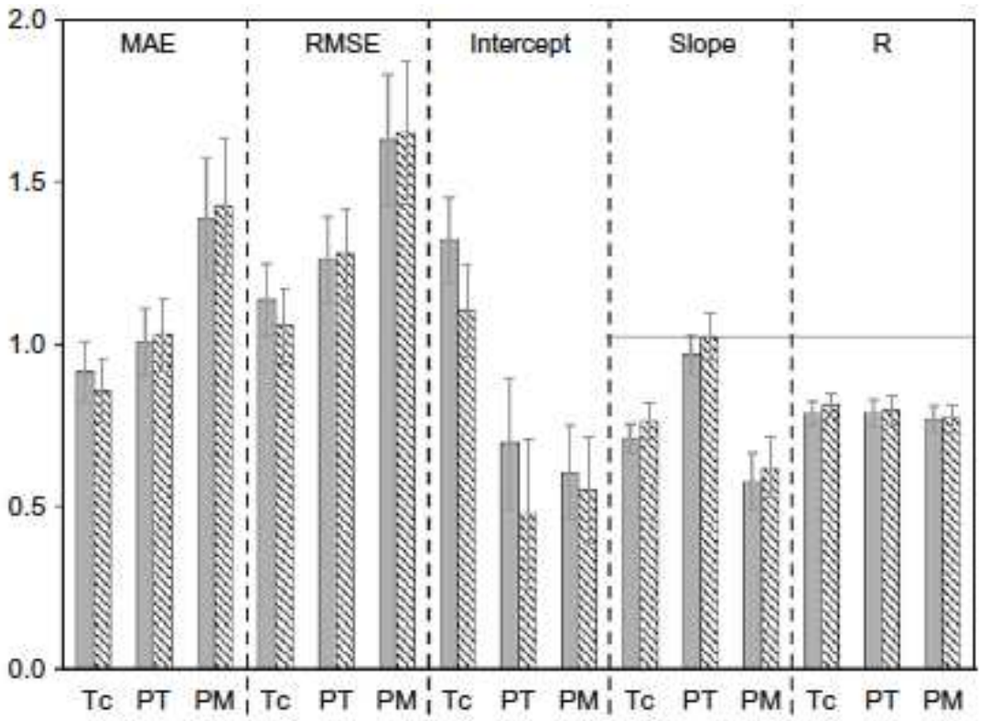

Fig. 4. From Douglas et al. (2009). Comparison of aggregate error statistics (in mm day^{-1}) mean absolute error (MAE), RMSE, Intercept, Slope, and regression coefficients (R), where Tc = Turc method; PT = Priestley–Taylor method; PM = Penman–Monteith method. Filled bars represent statistics computed on all "good" days, hashed bars represent statistic computed for days when the Bowen ratio (β) < 1. Mean values are represented by the heights of the bars. Error bars show the standard error of the mean. The horizontal line on Slope and R represents a value of 1.

The relative ranking of PET methods apparent in this study is (from best to worst): Priestley-Taylor, Turc, and Penman-Monteith, as shown in Fig. 4 (from Douglas et al. 2009). Performance at a daily time scale is indicated by the values of the regression intercept and slope and the correlation coefficient, R (or r). From Fig. 4, at a daily scale, the Turc intercept is much higher and statistically different than either the Priestley-Taylor or Penman-Monteith statistics. The Priestley–Taylor intercept statistics are closest to zero and slope and R statistics closest to 1. At a daily scale, the performance of all three methods does improve when applied to conditions close to PET (β ≤ 1). However, probably due to the lower sample size, the improved statistics are not significantly different from those computed for all ''good" data. Interestingly, R values for all models are nearly identical. In aggregate, the Turc and Priestley–Taylor methods perform comparably and both outperform the Penman-Monteith method. But at a daily scale, the Priestley–Taylor performance appears to be superior to the other two methods. In fact, the slope and intercept show that the Turc method significantly overestimates low DET values and underestimates high values. Hence, the Priestley–Taylor method appears to be the best model for estimating PET in Florida.

The Priestley-Taylor method used in this study to estimate PET requires direct measurements of R_N, or R_N derived from incoming solar radiation. As the ground-based

network of R_N instrumentation in Florida is sparse, an alternate method must be used for obtaining solar radiation to obtain statewide spatially distributed estimates of R_N and, therefore, PET. The GOES satellites are able to provide hourly estimates of solar radiation that are critical to PET calculations, and that have a spatial resolution that is significantly better than what is available from ground-based pyranometer networks.

5.2 Priestley-Taylor method

The Priestley-Taylor method estimates PET using the concept of the theoretical lower limit of evaporation from a wet surface as the "equilibrium" evaporation

$$PET_o = \alpha_{PT} \frac{\Delta}{\Delta + \gamma}\left(R_N - G\right), \tag{4}$$

where PET_o is the Priestley-Taylor-estimated PET (MJ m^{-2} d^{-1}), α_{PT} is the Priestley-Taylor coefficient, Δ is the slope of the saturation vapor pressure curve, γ is the psychrometric constant, R_N is the net radiation (MJ m^{-2} d^{-1}), and G is the soil heat flux (MJ m^{-2} d^{-1}). "Equilibrium" is defined here as evaporation from a wet surface under conditions of minimum advection that result in the actual vapor pressure of the air approaching the saturation vapor pressure. Priestley & Taylor (1972) showed that for conditions of minimum advection with no edge effects, α_{PT} = 1.26. For this project, the Priestley-Taylor equation was used with α_{PT} = 1.26 and, because daily PET computations were made, G was assumed to be negligible. Dividing PET in MJ m^{-2} d^{-1} by $\lambda\rho_w$ [λ is the latent heat of vaporization (MJ kg^{-1}), ρ_w is the density of water (= 1,000 kg m^{-3})] converts PET to a daily depth of water (mm).

The parameters Δ (kPa°C^{-1}) and γ (kPa°C^{-1}) were computed using

$$\Delta = \frac{4098 e_s}{(237.3 + T_{\min})^2} \tag{5}$$

$$\gamma = \frac{c_p P}{\varepsilon \lambda} \times 10^{-3} = 0.0016286 \frac{P}{\lambda}, \tag{6}$$

where e_s is the saturated vapor pressure (in kPa), c_p is the specific heat of moist air (1.013 kJ kg^{-1} °C^{-1}), P is atmospheric pressure (set equal to 101.3 kPa) and $T_{\min}$ is the minimum daily temperature (°C). Saturated vapor pressure was computed as

$$e_s = 0.6108 \exp\left(\frac{17.27 T_{\min}}{237.3 + T_{\min}}\right) \tag{7}$$

The latent heat of vaporization, $MJkg^{-1}$, is determined as

$$\lambda = 1000(2.501 - 0.002361T). \tag{8}$$

In addition, climate variables, solar radiation (R_s; $MJm^{-2}day^{-1}$), maximum ($T_{\max}$) and $T_{\min}$ daily temperatures (°C), and maximum ($RH_{\max}$) and minimum ($RH_{\min}$) daily relative humidities (%) are used directly and indirectly in the PET methodology, Eqs (4)-(8). The average temperature (T) is computed as the average of $T_{\max}$ and $T_{\min}$.

5.3 Estimating net radiation for PET computation

Jacobs et al. (2008) compared multiple methods of calculating R_N, the difference between downwelling and upwelling radiation of both short and long wavelengths, to identify the most robust method for Florida. The recommended method uses a four-component approach where incoming solar radiation, surface albedo, and upwelling and downwelling longwave (LW) radiation must each be measured or estimated. In the recommended method, R_N is estimated using

$$R_N = R_s(1-\alpha) + 0.0864\varepsilon_s R_{LWD} - 0.0864 R_{LWU}, \quad (9)$$

where R_s is the daily solar radiation ($MJm^{-2}day^{-1}$), α is the surface albedo, ε_s is the surface emissivity, R_{LWD} is the downwelling L radiation (Wm^{-2}), R_{LWU} is the upwelling LW radiation (Wm^{-2}), and 0.0864 is the conversion between Wm^{-2} and $MJm^{-2}day^{-1}$. R_N is determined from measured or estimated solar radiation, estimates of α, and modeled LW radiation values from ancillary meteorological data. For this project, the GOES R_s product is used to estimate R_s. Field measurements of downwelling LW, upwelling LW radiation, and reflected insolation were made by SJRWMD using Kipp & Zonen CNR1 sensors at 11 sites in SJRWMD during 2004-2005. The site land covers included water, wetland, urban, rangeland, forest, and agriculture. These radiation data were used to identify suitable methods to estimate the two LW radiation terms and the surface α (ratio of reflected insolation to incoming insolation) throughout Florida.

5.4 Estimating longwave radiation for PET computation

5.4.1 Downwelling longwave for PET computation

Estimation of downwelling LW radiation (R_{LWD}; Wm^{-2}) for PET computation requires two steps: 1) estimation of the clear sky radiation (R_{LWDc}) and 2) implementation of a correction for cloud cover. Choi et al. (2008) determined that R_{LWDc} is best estimated using the Sellers (1965) method (Eq. 10) with Florida-specific parameterization.

$$R_{LWDc} = (a_1 + a_2 e_a^{1/2})\,\sigma T^4, \quad (10)$$

where e_a is the (mean actual) atmospheric vapor pressure (mb), σ is the Stefan-Boltzman constant ($Wm^{-2}K^{-4}$), and T is the average air temperature (K). For this analysis, the Florida-specific coefficients a_1 and a_2 (0.575 and 0.054, respectively) are quite similar to Sellers' original values (0.605 and 0.048).

The vapor pressure, e_a (kPa), requires first calculating the saturation vapor pressure e_s (kPa), using Eq. (7). Then, the daily mean actual vapor pressure, e_a, is calculated from daily extreme temperature and relative humidity values using

$$e_a = \frac{e_s(T_{max})\frac{RH_{min}}{100} + e_s(T_{min})\frac{RH_{max}}{100}}{2}. \quad (11)$$

and converted from kPa to mb using a multiplier of 10. Choi et al. (2008) determined that the (Crawford and Duchon, 1999) method provides the best approach to obtain an equation that calculates daily downwelling LW under both clear and cloudy conditions. Specifically,

$$R_{LWD} = R_{LWDc}(1 - c) + c\sigma T^4, \quad (12)$$

where c is fractional cloud cover estimated from the incoming solar radiation (Crawford & Duchon, 1999) as

$$c = 1 - R_s/R_{so}, \quad (13)$$

where R_s is in this study the GOES-estimated incoming solar radiation at the surface, and R_{so} is from Eqs. (1) and (2).

5.4.2 Upwelling longwave for PET computation

Upwelling LW radiation is calculated using surface measurements of temperature

$$R_{LWU} = \varepsilon_s \sigma T_s^4 \quad (14)$$

where ε_s is the surface emissivity, σ is the Stefan-Boltzmann constant, and T_s is the surface temperature. Average daily air temperature (T) is used in Eq. (14) instead of T_s when estimates of daily temperature are needed (Brutsaert, 1982). For typical surfaces, ε_s is approximately 0.97 and this value was assumed in the present study.

5.5 Estimating surface albedo for PET computation

An important step in the four-component calculation of R_N is to estimate surface α accurately. Ultimately, each 2 km cell within the Statewide ET grid will require an α estimate. Three approaches were considered; using measured α values to provide estimates, estimating α using literature values by land use, and using MODerate Resolution Imaging Spectroradiometer (MODIS) or GOES remotely sensed data. A review of site-specific daily α measurements (from the 11 SJRWMD radiation sites) provides insight into typical values across Florida land uses. For all sites, values were mainly between 0.10 and 0.20. A much lower value, 0.062 was observed for an open water site. The highest and lowest average α values were found for a rangeland site and the water sites, respectively. Albedo values were not consistent within land uses. The α data showed differences in magnitude and temporal variability, even within the same land use type. These differences may reflect either the heterogeneous nature of some land uses, or the relatively small number of sites with four-component radiometer data within each land use type.

Most sites where four-component radiometer data were collected exhibited an annual cycle of α, with highest α in December and lowest in July. Differences between the low and high values were on the order of 0.05. The annual cycle was less pronounced for the citrus and forest sites. Apart from the annual cycle, day-to-day values are fairly consistent. Exceptions include a wetland area and an agricultural site. The wetland variation may be due to dynamic water levels that change the relative portion of water and vegetation at the surface. The agricultural site is likely influenced by crop growth and harvest. Because α values did not differ greatly across sites and no consistent values could be distinguished by land use, constant α values were considered to see if they provided reasonable estimates of R_N. Two constant α approaches were examined. One uses a single average α value determined from the mean measured values (0.141), and the other uses two α values determined from the mean measured values for land (0.149) and water (0.062).

The second approach considered to estimate α was to use literature values. Literature values typically were consistent with the measured data from Florida. However, literature values had

a range (0.10 to 0.20) that exceeded the entire range observed across measured sites, excluding water. Given the wide range of literature values, the measured α were evaluated further.

The third approach uses satellite-derived α values. Data from the MODIS satellite-borne sensors can be interpreted to provide α data at 16-day, 500-m resolution (Salomon et al., 2006). However, because the MODIS data are not available prior to December 1999 and the period of interest for this study begins in 1995 MODIS α was not considered further. GOES α values were derived as an intermediate product of the GDM, and was produced for the entire period of study at the same temporal resolution as solar radiation. To assess the validity of the GOES estimate, we compared it to sites with measured α that had consistent land cover over a large surrounding area, so that land use variation within the grid would be minimal. After examining satellite images of all the radiation sites, three sites were identified that had relatively homogeneous land cover conditions over at least a 2 km footprint (rangeland, forest, and agricultural land covers). The GOES product was found to consistently underestimate α compared to measured α, however the seasonal patterns appeared to be consistent. Thus, we conducted a linear regression analysis using measured values from the three sites and estimated scaled GOES α for 2005. The original GOES α product was improved by an average regression equation [$y = 0.634x+0.0679$, where y is the scaled GOES α, x is the original GOES α, and where correlation coefficient (r^2) values were <0.2]. The corrected GOES α was more suitable for estimating R_N. However, as a whole, the GOES α tends to create a 6% positive bias, while the constant α approach only slightly underestimate the measured R_N values. Overall, the constant α values therefore provided better R_N estimates than did the GOES α estimates. The bimodal α approach gives $r^2 = 0.93$, a RMSE of 16.0 Wm^{-2}, and a 2% negative bias, suggesting a very minor reduction in performance using a constant α rather than site specific values.

Based on the comparison of several α approaches described above, constant α values were used for land (0.149) and water (0.062) in computation of PET. The SJRWMD, in collaboration with SFWMD and the USGS, classified all the 2 km grid pixels in Florida as either land or water (Fig. 5). Inland pixels were identified as water if 75% or more of the pixel contained water. The Atlantic Ocean, Gulf of Mexico, lagoons and bays were not classified as water in Fig. 5, and are coded as land with α values of 0.149. The calculated PET values use a land α for these regions.

6. Estimating reference ET

For the purpose of establishing uniform ET estimates and transferable crop coefficients, the ASCE Evapotranspiration in Irrigation and Hydrology Committee (ASCE-ET) recommends two standardized reference ET surfaces: (1) a short crop (similar to grass) and (2) a tall crop (similar to alfalfa). Also recommended is one standardized RET equation based on the Penman-Monteith equation (Penman, 1948; Monteith, 1965; Allen et al., 1998). As a part of the standardization, the "full" form of the Penman-Monteith equation and associated equations for calculating aerodynamic and bulk surface resistance were combined and reduced to a single equation having two constants (see Allen et al., 1998).

For a grass reference on a daily basis, the RET (RET_o in Eq. 15) method is given as

$$RET_o = \frac{0.408\Delta(R_N - G) + \gamma \frac{900}{T+273} u_2 (e_s - e_a)}{\Delta + \gamma(1 + 0.34u_2)}, \quad (15)$$

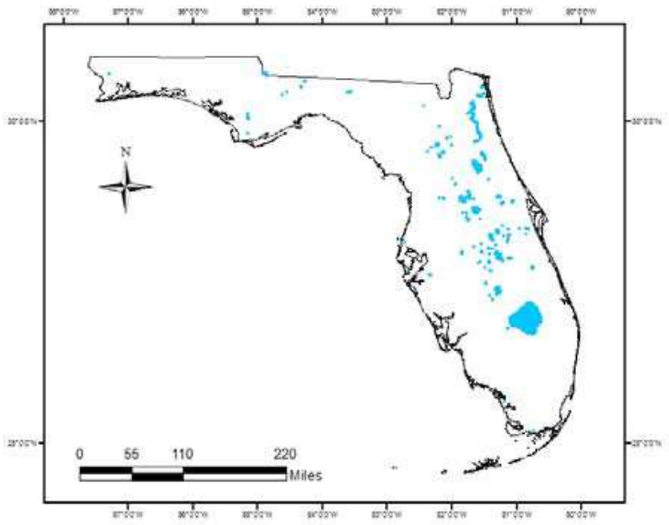

Fig. 5. Florida inland water bodies.

where the variables are as for Eqs. (4)-(8), T the average air temperature (°C), and while u_2 (ms^{-1}), e_a (kPa), and e_s–e_a (kPa) are defined below.

The standardized method used in this project is the short crop or grass reference calculated on a daily basis. This hypothetical reference surface has an assumed canopy height of 0.12 m, a constant bulk surface resistance of 70 sm^{-1}, and an assumed albedo of 0.23. The zero plane displacement height and roughness lengths are estimated as a function of the assumed crop height, so that aerodynamic resistance becomes a function of only the measured wind speed. The height for the temperature, humidity, and wind measurements is assumed to be 2 m. The latent heat of vaporization λ, is assigned a constant value of 2.45 MJkg^{-1}.

Wind speed values not collected at 2 m were converted to the 2-m height prior to calculating RET using the standard procedures outlined in the Food and Agriculture Organization of the United Nations Irrigation and Drainage Paper No. 56 (FAO56; Allen et al., 1998) according to the following equation:

$$u_2 = u_z \frac{4.87}{\ln(67.8z - 5.42)}, \tag{16}$$

where u_2 is the measured wind speed at z-meters above ground surface (ms^{-1}), in this case z=2, and z is the height of measurement above ground surface (m). The vapor pressure deficit requires the saturation vapor pressure, calculated in Eq. (7).

For this ASCE method, the daily mean saturation vapor pressure, e_s (kPa), is calculated as

$$e_s = \frac{e_s(T_{\max}) + e_s(T_{\min})}{2} \tag{17}$$

and the daily mean actual vapor pressure (kPa) is calculated from Eq. (11) (actual vapor pressure). R_N calculated using this ASCE method is the difference between net shortwave radiation (R_{nSW}) and net LW radiation (R_{nLW})

$$R_N = R_{nSW} - R_{nLW}. \tag{18}$$

Net shortwave radiation, R_{nSW}, is calculated the same as previously using insolation (R_s), with α=0.23:

$$R_{nSW} = (1-\alpha) R_s \,. \tag{19}$$

The R_{nLW} calculation is somewhat more involved. R_{nLW} is calculated as

$$R_{nLW} = \sigma \left[\frac{\left(T_{max,K}\right)^4 + \left(T_{min,K}\right)^4}{2} \right] \left(0.34 - 0.14\sqrt{e_a}\right) \left(1.35 \frac{R_s}{R_{so}} - 0.35\right), \tag{20}$$

where $T_{max,K}$ and $T_{min,K}$ are the maximum and minimum absolute temperatures (K) during the 24-hour period, extraterrestrial radiation, R_a, is calculated as in Eq. (2) from Julian day and latitude, and outgoing solar radiation, R_{so}, is calculated from:

$$R_{so} = 0.75 R_a \,. \tag{21}$$

Other terms are as defined previously.

7. Calibration influences on PET and RET, and ancillary meteorological data

Paech et al. (2009) provide a detailed analysis of the issues surrounding the calibration of the GOES insolation estimates. These issues include: (1) the change in GDM model bias with time (as a function of GOES visible sensor age since launch), and (2) less well known seasonal bias oscillations caused by sun angle, sun glint, and season aerosol concentrations (e.g., presence of the Saharan Air Layer over Florida in summer). However, one aspect that is particularly relevant for this analysis is how the GOES insolation errors, in terms of percentage, propagate into RET and PET estimates.

PET can be highly influenced by errors or variability in insolation because the computations are not offset by an aerodynamic component as with RET (Eq. 15). For example, in the Priestley-Taylor approach (Priestley & Taylor, 1972) used in this study (Eq. 4), PET is directly proportional to R_N, and because most of the variability in R_N is due to the insolation component, PET is particularly sensitive to that energy flux. From a preliminary analysis, it is estimated that a 10% error in insolation causes a 10-11% error in annual average PET and only a 6-7% error in annual average RET. Overall, monthly RET generally exceeds PET in the winter due to the often high winds during this season and the presence of wind speed in the aerodynamic term of the RET equation.

Lastly, the RET and PET calculations require ancillary daily meteorological data. Tables 1 and 2 summarize the required data and their sources. A quality assurance procedure was applied to measured data. A threshold analysis was applied to limit the maximum relative humidity to 100%. Temperature, relative humidity, and wind speed were assessed using graphical tools. The short periods having erroneous or missing values were replaced with an average of the previous and next day's values. Longer periods having erroneous or missing values were replaced with average recorded values using the remaining years' observations for that site and day. The gridded meteorological data are created from point station data. An inverse distance weighting method is used to interpolate daily point meteorological data to a 2 km grid scale on an annual basis for each meteorological variable. The five meteorological variables each require a separate interpolation.

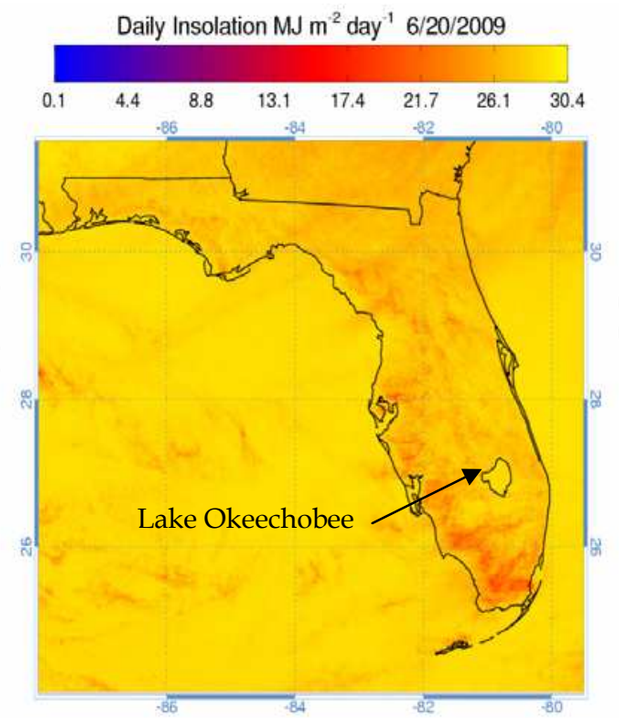

(a)

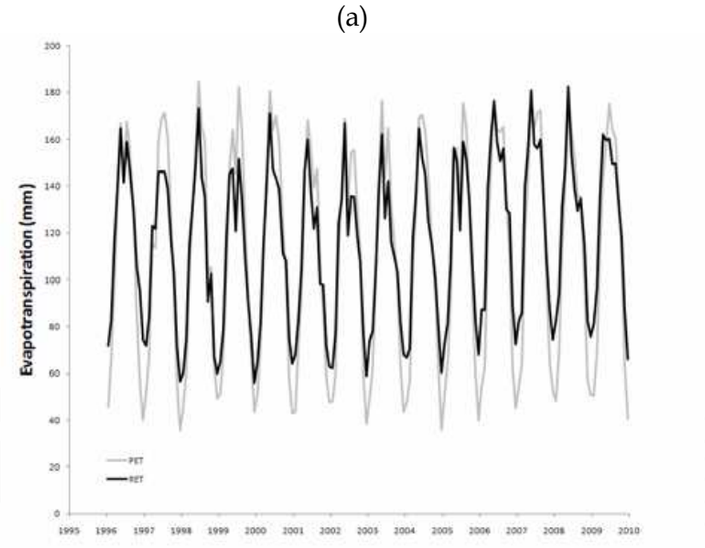

(b)

Fig. 6. (a): Daily insolation for 20 June 2009. (b): Estimated monthly PET and RET near Lake Starr in central Florida as estimated using the insolation data.

Figure 6a shows a map of the final product, 2 km daily insolation for one day (20 June 2009) developed from the calibrated GDM method using GOES satellite data. Note the spatial variation in the insolation in Fig. 6a resulting from differences in cloud cover across the State. The relatively clear-sky conditions over the ocean, near-coastal area, and the large inland Lake Okeechobee are features that produce persistent patterns in insolation. The variation of monthly PET and RET is seen in Figure 6b, exhibiting the substantial correlation

between these two ET values. Also, the year-to-year variation in PET and RET is apparent, largely related to similar variations in insolation.

Model Input	PET_o	RET_o	Source
Solar Radiation (mean)	X	X	GOES
Air Temperature (min and max)	X	X	NOAA/NCDC, FAWN
Relative Humidity (min and max)	X	X	NOAA/NCDC, WMDs, FAWN
Wind Speed (mean)		X	NOAA/NCDC, WMDs, FAWN
Incoming Longwave Radiation	X		Calculated using Air Temperature, Relative Humidity, and Insolation
Outgoing Longwave Radiation	X		Calculated using Air Temperature
Albedo	X		SJRWMD R_N Network Values
Land or Water	X		GIS Landcover Analysis

Table 1. Required input data sources by method.

Source	Full Name	Source
NOAA/NCDC	National Oceanic and Atmospheric Administration (NOAA) National Climate Data Center	http://www.ncdc.noaa.gov/oa/ncdc.html
FAWN	Florida Automated Weather Network	http://fawn.ifas.ufl.edu/data/reports/
SJRWMD	St. Johns River Water Management District	http://sjr.state.fl.us/data.html
SWFWMD	Southwest Florida Water Management District	http://www.swfwmd.state.fl.us/data/
SFWMD	South Florida Water Management District: DBHydro	http://www.sfwmd.gov/dbhydroplsql/show_dbkey_info.main_menu

Table 2. Web addresses for source data (effective November, 2007).

8. High-resolution ET products and applications across Florida

The spatially continuous PET and RET coverages of the entire State of Florida derived from GOES satellite data are presented and discussed in this section. Figure 7(a-d) illustrates an example for 2004: mean annual PET (Fig. 7a), mean July RET (Fig. 7b), mean annual RET (Fig. 7c), and insolation (Fig. 7d). Note that the continuity and high spatial resolution of these data are not attainable from ground-based observation networks. All data are plotted at 2 km resolution. The general north-to-south increase in PET and RET is seen in Figs. 7 (a and c), with the insolation map for July showing less variability as expected.

Figure 8(a-b) illustrates an example of daily PET and RET for 20 June 2009 over Florida. In this figure, the water bodies are seen clearly (see Fig. 5), especially in the PET map, because

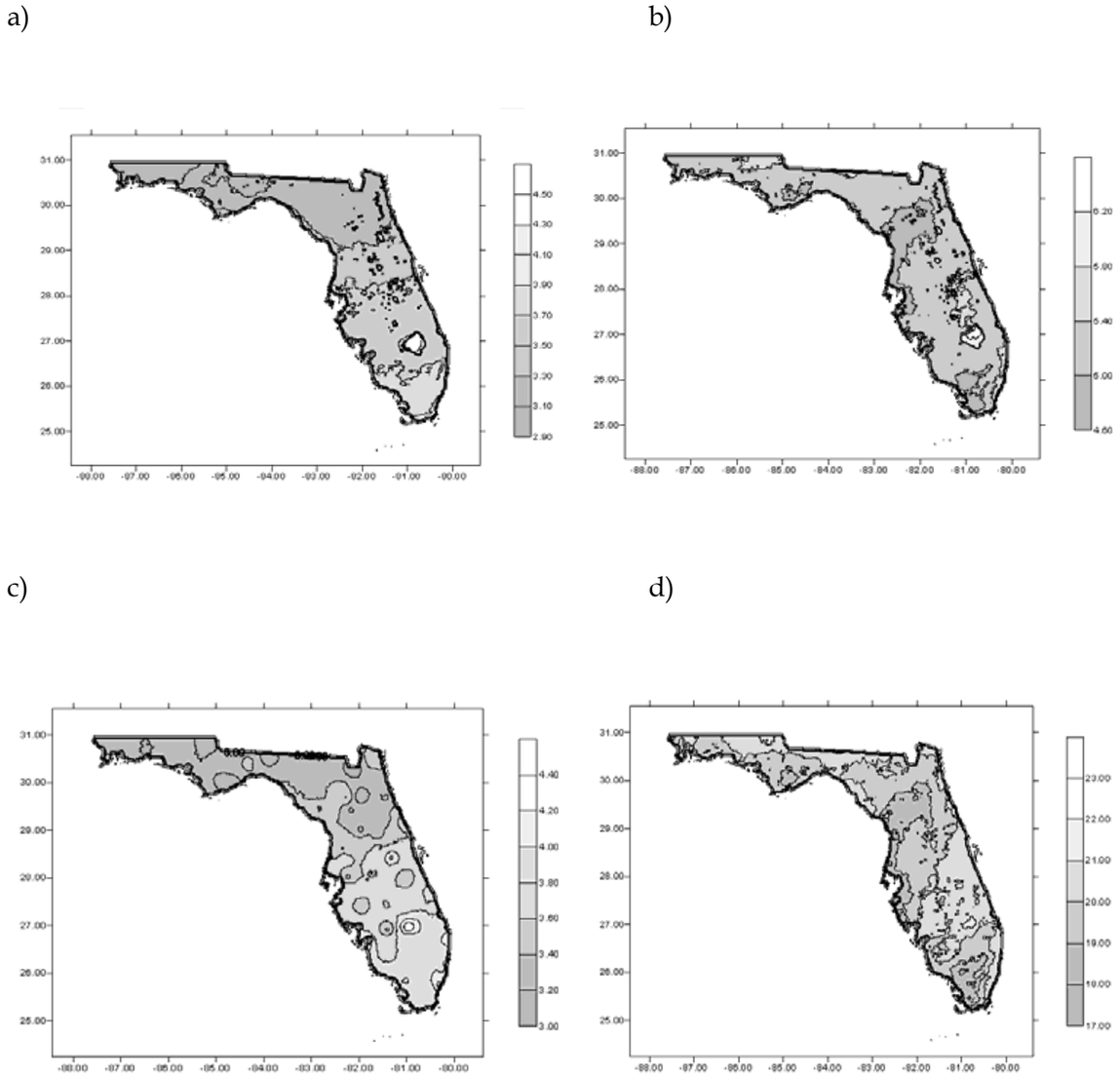

Fig. 7. (a) 2004 mean annual PET (mm day^{-1}), (b) mean July 2004 RET (mm day^{-1}), (c) 2004 mean annual RET (mm day^{-1}), (d) and insolation (MJ m^{-2} day^{-1}) for July 2004.

of the water/land variation in surface α used in the PET computation. In addition, the clear-sky conditions and associated high insolation (Fig. 6a) over the large inland Lake Okeechobee contribute to a distinct area of high PET and RET. The strong spatial correlation between insolation (Fig. 6a) and PET/RET (Fig. 8a-b) is indicative of the primary control of insolation on these ET values. The GOES insolation product is well suited to capture Statewide variations in this variable and the procedures outlined in this chapter present a viable approach to integrate this high-quality insolation product into computations of PET and RET.

This chapter has demonstrated how high resolution (2 km) insolation from GOES visible satellite data can be used to produce spatially uniform and continuous estimates of RET and PET over a statewide region. Florida, which experiences a wide range of ET conditions, has been a demonstration testbed for these products, which have proved to be valuable to the agricultural and hydrologic communities. These data also close the water budget by allowing for quality estimation of maximum evaporation and/or ET, which has been a difficult quantity to measure consistently over large regions. High-quality insolation data will be available from geostationary visible sensors for the long-term future, which allows any region within the view of a geostationary satellite (~55° N to ~55° S latitude) to develop a similar application.

Daily PET, RET insolation, and ancillary meteorological data for the State of Florida are processed and archived on an annual basis and are available at the USGS Florida Water Science Center Hydrologic Web Portal (hdwp.er.usgs.gov).

Use of trade, product, or firm names in this publication is for descriptive purposes only and does not imply endorsement by the U.S. Government.

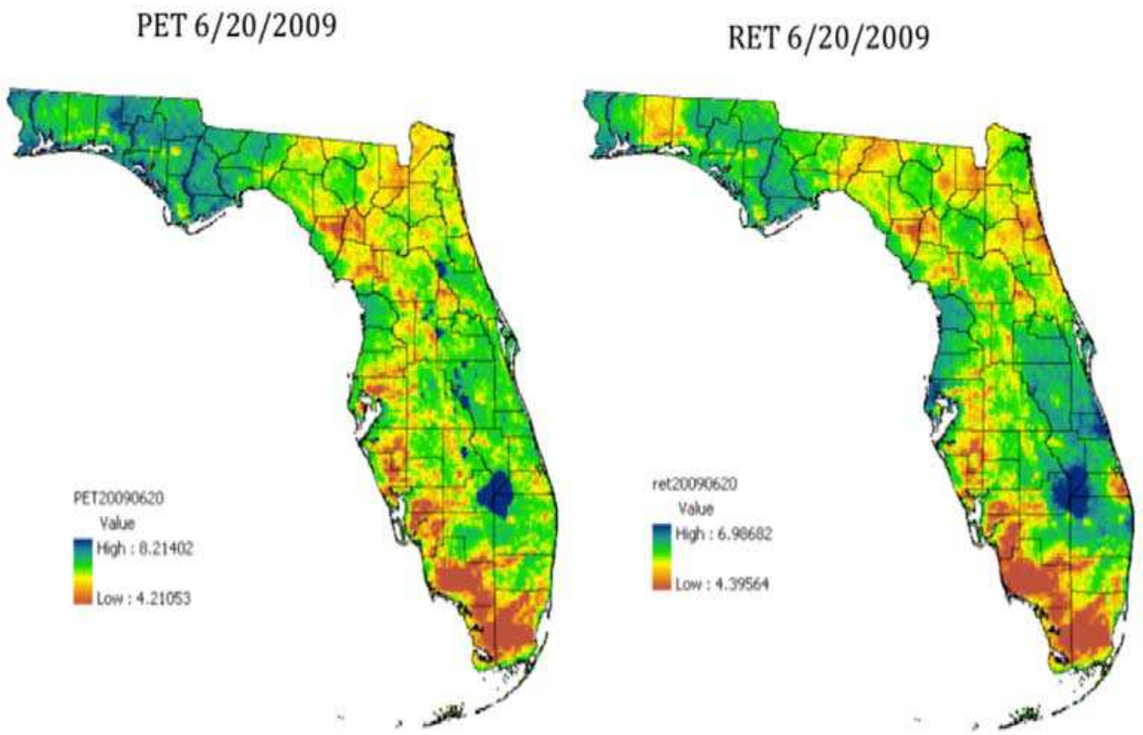

Fig. 8. Daily PET (mm day^{-1}; left) and RET (mm day^{-1}; right) for 20 June 2009. These images used the daily-integrated insolation as shown in Fig. 6a, and exemplify the high-resolution (2 km) detail that can be retrieved when GOES data are exploited in this manner.

9. References

Allen, R. G. (1996). Assessing integrity of weather data for use in reference evapotranspiration estimation. *J. Irrig. and Drain. Engrg*., ASCE. 122, 97-106.

Allen, R. G.; Periera, L. S., Raes D. & M. Smith (1998). Crop evapotranspiration: Guidelines for computing crop requirements. Irrigation and Drainage Paper No. 56. Rome, Italy: FAO.

Allen, R. G.; I. A. Walter, R. L. Elliott, T. A. Howell, D. Itenfisu, M. E. Jensen, & R.L. Snyder (2005). The ASCE standardized reference evapotranspiration equation, American Society of Civil Engineers, Reston, Virginia.

Anderson, M. C.; W. L. Bland, J. M. Norman & G. R. Diak (2001). Canopy wetness and humidity prediction using satellite and synoptic-scale meteorological observations, *Plant Dis*., 85, 1018–1026.

Anderson, M. C.; W. P. Kustas, & J. M. Norman (2003). Upscaling and downscaling — A regional view of the soil-plant-atmosphere continuum, *Agron. J*., 95, 1408–1432.

Anderson, M. C.; J. M. Norman, J. R. Mecikalski, R. D. Torn, W. P. Kustas, & J. B. Basara (2004). A multiscale remote sensing model for disaggregating regional fluxes to micrometeorological scales, *J. Hydrometeor*., 5, 343–363.

Brutsaert, W. (1982). *Evaporation into the Atmosphere – Theory, History and Application*. Kluwer Academic Publishers, Dordrecht.

Choi, M.; J. M. Jacobs, & W. P. Kustas (2008). Assessment of clear and cloudy sky parameterizations for daily downwelling longwave radiation over different land surfaces in Florida, USA, *Geophys. Res. Lett.*, 35, L20402, doi: 10.1029/2008GL035731.

Cosgrove, B. A.; D. Lohmann, K. E. Mitchell, P. R. Houser, E. F. Wood, J. Schaake, A. Robock, C. Marshall, J. Sheffield, L. Luo, Q. Duan, R. T. Pinker, J. D. Tarpley, R. W. Higgins, & J. Meng (2003). Realtime and retrospective forcing in the North American Land Data Assimilation Systems (NLDAS) project. *J. Geophys. Res*., 108 (D22), 8842, doi:10.1029/ 2002JD003118.

Cosgrove, B. A.; D. Lohmann, K. E. Mitchell, P. R. Houser, E. F. Wood, J. C. Schaake, A. Robock, J. Sheffield, Q. Duan, L. Luo, R. W. Higgins, R. T. Pinker, & J. D. Tarpley (2003). Land surface model spinup behavior in the North American Land Data Assimilation System (NLDAS). *J. Geophys. Res*., 108 (D22), 8845, doi:10.1029/2002JD003119.

Crawford, T. M. & C. E. Duchon (1999). An improved parameterization for estimating effective atmospheric emissivity for use in calculating daytime downwelling longwave radiation. *J. Appl. Meteorol*. 38, 474–480.

Darnell, W. L.; W. F. Staylor, S. K. Gupta, & F. M. Denn (1988). Estimation of surface insolation using sun-synchronous satellite data, *J. Climate*, 1, 820–835.

Dedieu, G.; P. Y. Deschamps, & Y. H. Kerr (1987). Satellite estimates of solar irradiance at the surface of the earth and of surface albedo using a physical model applied to meteosat data, *J. Climate Appl. Meteor*., 26, 79–87.

Diak, G. R. & C. Gautier (1983). Improvements to a simple physical model for estimating insolation from GOES data, *J. Climate Appl. Meteor*., 22, 505–508.

Diak, G. R.; W. L. Bland, & J. R. Mecikalski (1996). A note on first estimates of surface insolation from GOES-8 visible satellite data, *Agric. For. Meteor.*, 82, 219–226.

Diak, G. R.; M. C. Anderson, W. L. Bland, J. M. Norman, J. R. Mecikalski, & R. M. Aune (1998). Agricultural management decisions aids driven by real-time satellite data, *Bull. Amer. Meteor. Soc.*, 79, 1345–1355.

Douglas, E. M.; J. M. Jacobs, D. M. Sumner & R. L. Ray (2009). Potential evapotranspiration method selection for Florida land cover types. *J. Hydrology*. 373(3-4), 366-376.

Duffie, J. A. & W. A. Beckman (1980). *Solar Engineering of Thermal Processes*. John Wiley and Sons, New York, pp. 1-109.

Frouin, R.; C. Gautier, K. B. Katsaros, & J. Lind (1988). A comparison of satellite and empirical formula techniques for estimating insolation over the oceans, *J. Appl. Meteor.*, 27, 1016–1023.

Frouin, R. & B. Chertock (1992). A technique for global monitoring of net solar irradiance at the ocean surface. Part I: Model, *J. Appl. Meteor.*, 31, 1056–1066.

Gautier, C.; G. R. Diak, & S. Masse (1980). A simple physical model to estimate incident solar radiation at the surface from GOES satellite data, *J. Appl. Meteor.*, 19, 1007–1012.

Gautier, C.; G. R. Diak, & S. Masse (1984). An investigation of the effects of spatially averaging satellite brightness measurements on the calculation of insolation, *J. Climate Appl. Meteor.*, 23, 1380–1386.

Hoblit, B. C.; C. Castello, L. Liu, & D. Curtis (2003). Creating a seamless map of gage-adjusted radar rainfall estimates for the State of Florida, paper presented at EWRI World Water and Environmental Congress, Philadelphia, Pennsylvania, 23-26 June.

Jacobs, J.; J. Mecikalski, & S. Paech (2008). Satellite-based solar radiation, net radiation, and potential and reference evapotranspiration estimates over Florida. A Technical Report prepared for the State of Florida Water Management Districts. Available online at: hdwp.er.usgs.gov/ET/ GOES_FinalReport.pdf.

Jacobs, J. M.; D. A. Myers, M. C. Anderson, & G. R. Diak (2002). GOES surface insolation to estimate wetlands evapotranspiration, *J. Hydrol.*, 56, 53–65.

Jacobs, J. M.; M. C. Anderson, L. C. Friess, & G. R. Diak (2004). Solar radiation, longwave radiation and emergent wetland evapotranspiration estimates from satellite data in Florida, USA, *Hydrological Sci. J.*, 49, 461-476.

Mecikalski, J. M.; G. R. Diak, M. C. Anderson, & J. M. Norman (1999). Estimating fluxes on continental scales using remotely sensed data in an atmosphere–land exchange model, *J. Appl. Meteor.*, 38, 1352–1369.

Meng, C. J.; Pinker, R. T., Tarpley, D. J., & I. Laszlo (2003). A satellite approach for estimating regional land surface energy budget for GCIP/GAPP. *J. Geophys. Res.*, 108, D22, 8861, 10.1029/2002JD003088.

Monteith, J. L. (1965). Evaporation and environment. pp. 205-234. In G.E. Fogg (ed.) *Symposium of the Society for Experimental Biology, The State and Movement of Water in Living Organisms*, 19, Academic Press, Inc., NY.

Möser, W. & E. Raschke (1984). Incident solar radiation over Europe from METEOSAT data, *J. Climate Appl. Meteor.*, 23, 166–170.

Otkin, J.; M. C. Anderson, J. R. Mecikalski & G. R. Diak (2005). Validation of GOES-Based insolation estimates using data from the United States Climate Reference Network. *J. Hydrometeorol.*, 6, 475-640.

Oudin, L., C.; Michel, & F. Anctil (2005). Which potential evapotranspiration input for a lumped rainfall–runoff model? Part 1 – Can rainfall–runoff models effectively handle detailed potential evapotranspiration inputs? *J. Hydrology*, 303, 275–289.

Paech, S. J.; J. R. Mecikalski, D. M. Sumner, C. S. Pathak, Q. Wu, S. Islam, & T. Sangoyomi (2009). Satellite-based solar radiation in support of potential and reference evapotranspiration estimates over Florida: A 10-year climatology. *Water. Resources. Res.*, 45(6), 1328-1342.

Penman, H. L. (1948). Natural evaporation from open water, bare soil and grass. *Proc. Roy. Soc.* London A(194), S. 120-145.

Pinker, R. T. & J. A. Ewing (1985). Modeling surface solar radiation: Model formulation and validation, *J. Climate Appl. Meteor.*, 24, 389–401.

Pinker, R. T. & I. Laszlo (1992). Modeling surface solar irradiance for satellite applications on global scale, *J. Appl. Meteor.*, 31, 194–211.

Pinker, R. T.; R. Frouin, & Z. Li (1995). A review of satellite methods to derive surface shortwave irradiance, *Remote Sens. Environ.*, 51, 105–124.

Priestley, C. H. B. & Taylor, R. J. (1972). On the assessment of surface heat flux and evaporation using large-scale parameters. *Mon. Wea. Rev.*, 100, 81–92

Raphael, C. & J. E. Hay (1984). An assessment of models which use satellite data to estimate solar irradiance at the Earth's surface, *J. Climate Appl. Meteor.*, 23, 832–844.

Salomon, J. G.; C. B. Schaaf, A. H. Strahler, F. Gao, & Y. Jin. (2006). Validation of the MODIS bidirectional reflectance distribution function and albedo retrievals using combined observations from the Aqua and Terra platforms. *IEEE Transactions on Geoscience and Remote Sensing*, 44, 1555-1565, doi:10.1109/TGRS.2006.871564.

Schmetz, J. (1989). Towards a surface radiation climatology. Retrieval of downward irradiance from satellites, *Atmos. Res.*, 23, 287–321.

Sellers, W. D. (1965). *Physical Climatology*. University of Chicago Press, Chicago, Ill.

Stewart, J. B., C. J. Watts, J. C. Rodriguez, H. A. R. De Bruin, A. R. van den Berg, & J. Garatuza-Payan, 1999: Use of satellite data to estimate radiation and evaporation for northwest Mexico, *Agric. Water Manage.*, 38, 181–193.

Sumner, D. M. (2001). Evapotranspiration from a cypress and pine forest subjected to natural fires in Volusia County, Florida, 1998-99: U.S. Geological Survey WRIR 01-4245, 55 p.

Swancar, A.; T. M. Lee, & T. M. O'Hare (2000). Hydrogeologic setting, water budget, and preliminary analysis of ground-water exchange at Lake Starr, a seepage lake in Polk County, Florida: U.S. Geological Survey WRIR 00-4030, 65 p.

Tarpley, J. D. (1979). Estimating incident solar radiation at the surface from geostationary satellite data, *J. Appl. Meteor.*, 18, 1172–1181.

Vörösmarty, C. J.; C. A. Federer., & A. L. Schloss (1998). Potential evaporation functions compared on US watersheds: Possible implications for global-scale water balance and terrestrial ecosystem modeling. *J. Hydrology*, 207, 147–169.

Weymouth, G., & J. LeMarshall (1999). An operational system to estimate global solar exposure over the Australian region from satellite observations, *Aust. Meteor. Mag.*, 48, 181–195.

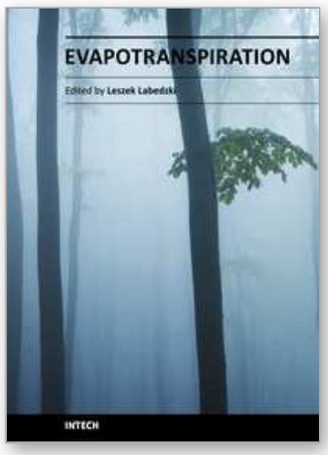

Evapotranspiration

Edited by Prof. Leszek Labedzki

ISBN 978-953-307-251-7
Hard cover, 446 pages
Publisher InTech
Published online 16, March, 2011
Published in print edition March, 2011

Evapotranspiration is a very complex phenomenon, comprising different aspects and processes (hydrological, meteorological, physiological, soil, plant and others). Farmers, agriculture advisers, extension services, hydrologists, agrometeorologists, water management specialists and many others are facing the problem of evapotranspiration. This book is dedicated to further understanding of the evapotranspiration problems, presenting a broad body of experience, by reporting different views of the authors and the results of their studies. It covers aspects from understandings and concepts of evapotranspiration, through methodology of calculating and measuring, to applications in different fields, in which evapotranspiration is an important factor. The book will be of benefit to scientists, engineers and managers involved in problems related to meteorology, climatology, hydrology, geography, agronomy and agricultural water management. We hope they will find useful material in this collection of papers.

InTech Europe
University Campus STeP Ri
Slavka Krautzeka 83/A
51000 Rijeka, Croatia
Phone: +385 (51) 770 447
Fax: +385 (51) 686 166
www.intechopen.com

InTech China
Unit 405, Office Block, Hotel Equatorial Shanghai
No.65, Yan An Road (West), Shanghai, 200040, China
中国上海市延安西路65号上海国际贵都大饭店办公楼405单元
Phone: +86-21-62489820
Fax: +86-21-62489821

IntechOpen